J. Am. Soc. Mass Spectrom. (2016) 27:1989–1998
DOI: 10.1007/s13361-016-1481-2

RESEARCH ARTICLE

Gas Phase Reactions of Ions Derived from Anionic Uranyl Formate and Uranyl Acetate Complexes

Evan Perez,[1] Cassandra Hanley,[1] Stephen Koehler,[1] Jordan Pestok,[1,3] Nevo Polonsky,[2] Michael Van Stipdonk[1]

[1]Department of Chemistry and Biochemistry, Duquesne University, 600 Forbes Ave., Pittsburgh, PA 15282, USA
[2]Chemistry Department, Bates College, Lewiston, Maine 04240, USA
[3]*Present Address:* Sto-Rox High School, McKees Rocks, PA 15136, USA

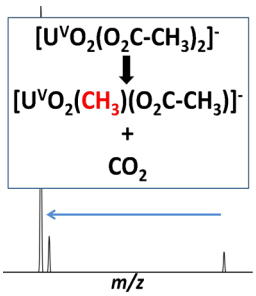

Abstract. The speciation and reactivity of uranium are topics of sustained interest because of their importance to the development of nuclear fuel processing methods, and a more complete understanding of the factors that govern the mobility and fate of the element in the environment. Tandem mass spectrometry can be used to examine the intrinsic reactivity (i.e., free from influence of solvent and other condensed phase effects) of a wide range of metal ion complexes in a species-specific fashion. Here, electrospray ionization, collision-induced dissociation, and gas-phase ion-molecule reactions were used to create and characterize ions derived from precursors composed of uranyl cation ($U^{VI}O_2^{2+}$) coordinated by formate or acetate ligands. Anionic complexes containing $U^{VI}O_2^{2+}$ and formate ligands fragment by decarboxylation and elimination of CH_2=O, ultimately to produce an oxo-hydride species $[U^{VI}O_2(O)(H)]^-$. Cationic species ultimately dissociate to make $[U^{VI}O_2(OH)]^+$. Anionic complexes containing acetate ligands exhibit an initial loss of acetyloxyl radical, CH_3CO_2•, with associated reduction of uranyl to $U^{V}O_2^{+}$. Subsequent CID steps cause elimination of CO_2 and CH_4, ultimately to produce $[U^{V}O_2(O)]^-$. Loss of CH_4 occurs by an intra-complex H^+ transfer process that leaves $U^{V}O_2^{+}$ coordinated by acetate and acetate enolate ligands. A subsequent dissociation step causes elimination of CH_2=C=O to leave $[U^{V}O_2(O)]^-$. Elimination of CH_4 is also observed as a result of hydrolysis caused by ion-molecule reaction with H_2O. The reactions of other anionic species with gas-phase H_2O create hydroxyl products, presumably through the elimination of H_2.

Keywords: Uranyl ion, Tandem mass spectrometry, Collision-induced dissociation, Acetate, Formate

Received: 14 July 2016/Revised: 6 August 2016/Accepted: 8 August 2016/Published Online: 7 September 2016

Introduction

The speciation and reactivity of uranium are topics of sustained interest [1] because of their importance to the development of nuclear fuel processing methods [2] and a more complete understanding of the factors the govern the mobility and fate of the element in the environment [3, 4]. Electrospray ionization (ESI) provides easy access to a wide range of gas-phase complexes containing uranium in high oxidation states (+5 and +6) for studies of intrinsic structure and reactivity (i.e., outside of the influence of solvent or other condensed phase effects) in a species specific fashion. For example, the transfer of uranium as mono-positive, pentavalent $U^{V}O_2^{+}$ from solution to the gas phase using ESI was first reported in 1992 [5] and since then, advances in the fundamental understanding of uranyl coordination chemistry have been made using the ionization method [6–21]. Most importantly, ESI has been used to generate gas-phase, doubly charged complexes containing UO_2^{2+}, such as $[UO_2(L)_n]^{2+}$, with L = acetonitrile (acn) or acetone (aco) and n = 4 or 5, for collision-induced dissociation (CID) and ion-molecule reaction experiments using tandem mass spectrometry [15].

ESI and tandem mass spectrometry have also been used to explore the intrinsic dissociation and ion-molecule reactions of transuranics [22–25]. For example, ESI was used to generate acn and aco complexes of PuO_2^{2+} and UO_2^{2+} solutions using similar experimental conditions [24]. In accord with relative stabilities of the actinyl ions, $UO_2^{2+} > PuO_2^{2+} > NpO_2^{2+}$, the yields of

Electronic supplementary material The online version of this article (doi:10.1007/s13361-016-1481-2) contains supplementary material, which is available to authorized users.

Correspondence to: Michael Stipdonk; *e-mail:* vanstipdonkm@duq.edu

plutonyl complexes with acn or aco were significantly lower than those of uranyl, and dipositive neptunyl complexes were not observed. CID of the di-positive coordination complexes in a 3-D quadrupole ion trap produced doubly and singly charged fragment ions; the fragmentation products revealed differences in underlying chemistries of PuO_2^{2+} and UO_2^{2+}, including the lower stability of Pu(VI) compared with U(VI).

Recently, gas-phase organoactinyl complexes were synthesized in an ion trap by collisional activation of anionic $An^{VI}O_2$ complexes where An = U, Np, Pu [26]. In these precursors, the formally $An^{VI}O_2^{2+}$ actinyl core was coordinated by three carboxylate ligands, with R = CH_3 (methyl), C≡C-CH_3 (butynl), C_6H_5 (phenyl), or C_6F_5 (pentafluorophenyl). One CID pathway observed for these precursor ions was decarboxylation to generate $[(R)AnO_2(O_2C\text{-}R)_2]^-$ products that presumably feature discrete An-C bonds. Isolation of the $[(R)AnO_2(O_2C\text{-}R)_2]^-$ products and subsequent reaction with gas-phase H_2O causes hydrolysis to generate species with composition $[AnO_2OH(O_2C\text{-}R)_2]^-$. The hydrolysis reactions provided support for the hypothesis that true organoactinyl species were generated.

Here we report the fragmentation of anionic uranyl complexes with general formula $[UO_2(O_2C\text{-}R)_3]^-$, R = H (formate) and CH_3 (acetate), in a linear ion trap (LIT) mass spectrometer. We have recently reported that the use of the 2-D ion trap provides access to fragmentation pathways and reactions not observed in earlier studies with 3-D ion traps. For example, our past studies of the dissociation behavior of gas-phase actinyl complexes using a 3-D ion trap were complicated by a preponderance of product ions obviously generated by interactions with background H_2O. Collisions with H_2O in the ion trap create hydrated product ions or led to charge reduction reactions that form $[UO_2OH]^+$ and $[UO_2]^+$ and complexes containing these cations [15, 16, 24]. In a prior CID study of acetone-coordinated UO_2^{2+}, ligand addition reaction rates were so fast that complexes with 2 or 3 coordinating aco ligands hydrated to generate heterogeneous, tetra-, or pentacoordinate complexes [15]. As a consequence, gas-phase complex ions containing UO_2^{2+} and two or fewer ligands could not be generated by CID in a "top-down" approach.

However, in a recent investigation of the fragmentation behavior of UO_2^{2+} complexes containing acn [27], we showed that the amount of adventitious H_2O in the LIT is significantly lower than in the 3-D ion trap employed in our previous studies. CID was used to drive complete acn ligand elimination to generate UO_2^{2+}, and this was the first reported generation of the bare di-cation by multiple-stage CID. More importantly, CID of $[UO_2(acn)]^{2+}$ generated $[UO_2NC]^+$, which subsequently fragmented to produce NUO^+. While the bare NUO^+ ion, which is isoelectronic with UO_2^{2+}, had previously been prepared in a "bottom-up" approach by insertion of U^+ into NO in an ion-molecule reaction [28], our experiments demonstrated that the species can also be created in a CID reaction. Formation of the nitrido species by transfer of N from cyanide was confirmed using precursors labeled with ^{15}N, and a mechanism involving a cyanate intermediate was proposed based on density functional theory (DFT) calculations. Similar experiments have now been conducted with aco-coordinated UO_2^{2+}, and novel products such as $[UO_2\text{-}HCO]^+$ and $[UO_2\text{-}CH_2CH_3]^+$ have been identified using a combination of isotope labeling and high-resolution/high accuracy mass measurements [29].

Our goal in this study was to map out more thoroughly the dissociation behavior of formate- and acetate-coordinated UO_2^{2+}, and the reactions of dissociation products with background H_2O in the LIT. To the best of our knowledge, the dissociation behavior of $[UO_2(O_2C\text{-}H)_3]^-$ has not yet been reported. CID of $[UO_2(O_2C\text{-}CH_3)_3]^-$ in a 3-D quadrupole ion trap has been reported [26, 30], and the structure of the species has been determined using infrared multiple-photon photodissociation (IRMPD) spectroscopy [31]. However, the experiments reported here demonstrate that the chemistry of product ions from both systems can be explored more accurately in the 2-D LIT. As discussed below, our results clear up some ambiguity in the intrinsic dissociation pathways for the uranyl–acetate complex [30], and reveal some apparent product ions that are better described as products of reactions with background H_2O.

Experimental

Samples of uranyl formate, d_1-formate, acetate, and d_3-acetate were prepared by combining ca. 2–3 mg of UO_3 (Strem Chemicals, Newburyport, MA, USA), corresponding to approximately 7×10^{-6} to 1×10^{-5} moles, with a 2-fold mole excess of the respective acids (purchased from Sigma Aldrich, St. Louis, MO, USA) and 400 μL of deionized/distilled H_2O contained in a glass scintillation vial. The solutions were allowed to incubate on a hot plate at 70 °C for 12 h. We chose to synthesize the compounds because uranyl formate (native or d-labeled) and uranyl d_3-acetate are not commercially available. *Caution*: *uranium oxide is radioactive* (*α- and γ-emitter*), *and proper shielding*, *waste disposal*, *and personal protective gear should be used when handling the material*.

When cooled, 20 μL of the resulting solution was diluted with 800 μL of 50:50 (by volume) H_2O/EtOH and used without further work-up as the spray solution for ESI-MS. Ethanol was used for these experiments to avoid any ambiguity when looking for potential molecular O_2 adducts to product ions [32–35]. With the limited mass measurement accuracy of the LIT, O_2 and CH_3OH adducts cannot be distinguished.

ESI and CID experiments were performed on a ThermoScientific (San Jose, CA, USA) LTQ-XL LIT mass spectrometer. The uranyl-carboxylate spray solutions were infused into the ESI-MS instrument using the incorporated syringe pump at a flow rate of 5 μL/min. In the negative ion mode, the atmospheric pressure ionization stack settings for the LTQ (lens voltages, quadrupole, and octopole voltage offsets, etc.) were optimized for maximum transmission of the singly-charged ions $[UO_2(O_2C\text{-}R)_3]^-$, R = H, D, CH_3, or CD_3, to the ion trap mass analyzer by using the auto-tune routine within the LTQ Tune program. In the positive ion mode, the transmission was optimized using

$[UO_2(O_2C\text{-}R)(CH_3CH_2OH)_2]^+$. Helium was used as the bath/buffer gas to improve trapping efficiency and as the collision gas for CID experiments.

For CID, precursor ions were isolated using an isolation width of 1.0 to 1.5 mass to charge (*m/z*) units. The exact value was determined empirically to provide maximum ion intensity while ensuring isolation of a single isotopic peak. To probe CID behavior in general, the (mass) normalized collision energy (NCE, as defined by ThermoScientific) was set between 5% and 18%, which corresponds to 0.075–0.27 V applied for CID with the current instrument calibration. The activation Q, which defines the frequency of the applied radio frequency potential, was set at 0.30 and the activation time employed was 30 ms.

To probe gas-phase reactions of selected precursor ions with background H_2O, ions were isolated using widths of 2–4 *m/z* units. The specific width used was chosen empirically to ensure maximum ion isolation efficiency. The ions were then stored in the LIT for periods ranging from 1 ms to 10 s. Despite the lower H_2O levels in the 2-D ion trap, there is still a sufficient partial pressure of the neutral to permit an investigation of ion-molecule reactions, particularly when using long isolation times. For both CID and ion-molecule reaction experiments, the mass spectra displayed represent the accumulation and averaging of at least 30 isolation, dissociation, and ejection/detection steps.

Results and Discussion

Tandem MS of $[UO_2(O_2C\text{-}H)_3]^-$

The ESI mass spectrum generated from uranyl formate in H_2O/CH_3CH_2OH is shown in Figure 1a. The dominant negative ion created by ESI was $[U^{VI}O_2(O_2C\text{-}H)_3]^-$ at *m/z* 405, and larger clusters containing UO_2^{2+} and formate were also observed. CID of the larger clusters generated $[U^{VI}O_2(O_2C\text{-}H)_3]^-$ (data not shown) as the dominant product and was not examined in detail.

The multiple-stage (MS^n) CID spectra generated by initially isolating $[U^{VI}O_2(O_2C\text{-}H)_3]^-$ at *m/z* 405 are shown in Figure 1b–d. Data generated using deuterium-labeled formic acid (HO_2C-D) are provided in Supplementary Figure S1a–c of the Supporting Information. The two product ions generated by CID of $[U^{VI}O_2(O_2C\text{-}H)_3]^-$ (MS/MS stage, Figure 1b) appeared at *m/z* 361 and 331. Owing to the low-mass cut-off of the of the LIT, we were not able to determine the extent to which $[U^{VI}O_2(O_2C\text{-}H)_3]^-$ dissociates to create formate at *m/z* 45.

As discussed below, the peak at *m/z* 331 is a product generated by dissociation of the ion at *m/z* 361. The ion at *m/z* 361 peak is likely formed by elimination of CO_2 and hydride transfer to $U^{VI}O_2^{2+}$ to generate a species with formula $[U^{VI}O_2(H)(O_2C\text{-}H)_2]^-$ via Reaction 1.

$$\left[U^{VI}O_2(O_2C{-}H)_3\right]^- \rightarrow \left[U^{VI}O_2(H)(O_2C{-}H)_2\right]^- + CO_2 \quad (1)$$

The loss of 44 mass units was also observed for CID of $[U^{VI}O_2(O_2C\text{-}D)_3]^-$ (MS/MS stage, Supplementary Figure S1a),

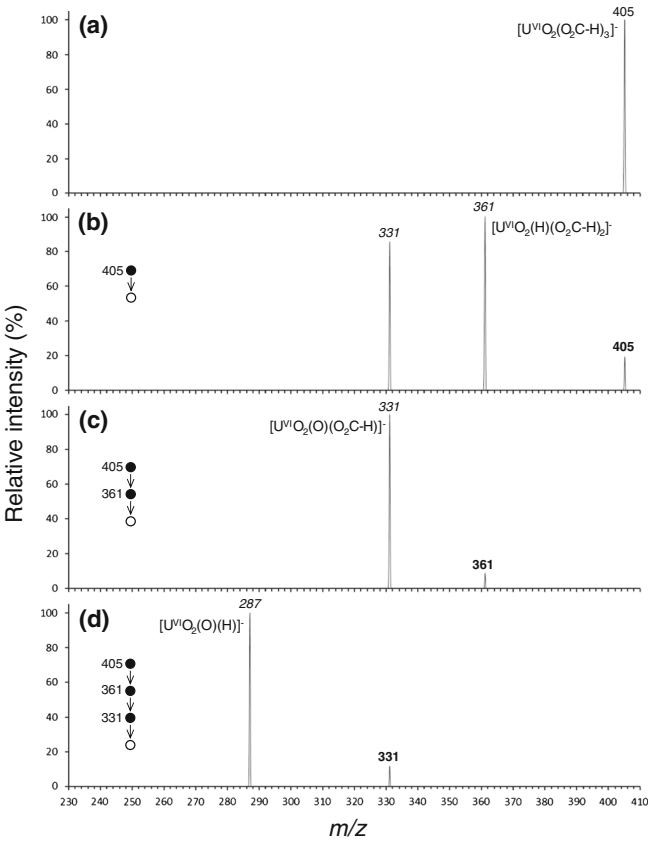

Figure 1. Negative ESI and CID spectra derived from uranyl formate in 50/50 H_2O/CH_3CH_2OH: (**a**) Full ESI spectrum, (**b**) CID of $[U^{VI}O_2(O_2C\text{-}H)_3]^-$ at *m/z* 405, (**c**) CID (MS^3 stage) of $[U^{VI}O_2(H)(O_2C\text{-}H)_2]^-$ at *m/z* 361, and (**d**) CID (MS^4 stage) of $[U^{VI}O_2(O)(O_2C\text{-}H)]^-$ at *m/z* 331. In the spectra, the circles and arrows illustrate the MS^n pathway. In each spectrum, the bold peak label indicates the precursor selected for CID whereas labels in italics represent the products from dissociation or ion-molecule reactions as indicated in the text

with transfer of D^- to the $U^{VI}O_2^{2+}$ core. Unlike previous reports [26, 30] of the dissociation behavior of uranyl-acetate anion ($[U^{VI}O_2(O_2C\text{-}CH_3)_3]^-$), elimination of formyloxyl radical, $\bullet O_2C\text{-}H$, with associated reduction of uranyl ion to the U(V) dioxo cation, $U^VO_2^+$, was not observed. The electron affinities (EA) of both formyloxyl radical [36, 37] and acetyloxyl radical [38] have been measured using negative ion photoelectron/photodetachment spectroscopy. The apparent lack of reduction/radical elimination for the uranyl-formate anion precursor is consistent with the higher EA of formyloxyl radical relative to acetyloxyl radical (3.498 ± 0.0015 eV and 3.250 ± 0.010 eV, respectively).

For CID of the $[U^{VI}O_2(H)(O_2C\text{-}H)_2]^-$ ion at *m/z* 361 (MS^3 stage, Figure 1c), the only product ion detected appeared at *m/z* 331. The neutral loss at this stage is 30 mass units, likely $CH_2{=}O$, and the product ion composition is assigned as $[U^{VI}O_2(O)(O_2C\text{-}H)]^-$. The dissociation reaction would, therefore, involve heterolytic cleavage of a formate C–O bond, retention of O^{2-} and hydride-transfer to create the neutral $O{=}CH_2$ neutral species as shown in Reaction 2. The neutral

loss shifted from 30 to 32 units following CID of $[U^{VI}O_2(D)(O_2C\text{-}D)_2]^-$ (MS^3 stage, Supplementary Figure S1b), consistent with the pathway depicted in Reaction 2.

$$\left[U^{VI}O_2(H)(O_2C{-}H)_2\right]^- \rightarrow \left[U^{VI}O_2(O)(O_2C{-}H)\right]^- + O{=}CH_2 \quad (2)$$

Subsequent CID of the ion at *m/z* 331 (MS^4 stage, Figure 1d) caused elimination of 44 mass units (CO_2) to create a product ion at *m/z* 287 $[U^{VI}O_2(O)(H)]^-$. To maintain an overall –1 charge on the product ion, we propose that the anion at *m/z* 287 is $[U^{VI}O_2(O)(H)]^-$, that is, $U^{VI}O_2^{2+}$ coordinated by oxide and hydride ligands. The loss of 44 units (CO_2), and a shift of the product ion *m/z* value to 288, was observed following CID of the deuterium labeled precursor $[U^{VI}O_2(O)(O_2C\text{-}D)]^-$ (MS^3 stage, Supplementary Figure S2c).

To probe the general reactions with H_2O in the LIT, we isolated the respective product ions generated by multiple stage CID of $[U^{VI}O_2(O_2C\text{-}H)_3]^-$ for periods ranging from 1 ms to 10 s. The product ion spectra generated by isolation and storage of $[U^{VI}O_2(O)(H)]^-$ at *m/z* 287 (the final product ion observed in Figure 1d) are shown in Figure 2. No adduct species were observed when $[U^{VI}O_2(O)(H)]^-$ was allowed to react with H_2O for 1 or 10 ms (Figure 2a and b). At 100 ms isolation time (Figure 2c), a product ion at *m/z* 303 appeared, and the same ion was the base peak at 1 s isolation time (Figure 2d). At 10 s isolation time, a product ion at *m/z* 321 dominated the spectrum (Figure 2e).

The *m/z* 303 product in Figure 2c and d is 16 mass units greater than the *m/z* 287 precursor, and we attribute this peak to the formation of $[U^{VI}O_2(O)(OH]^-$ by a process that involves H_2O addition and H_2 elimination, as shown in Reaction 3.

$$\left[U^{VI}O_2(O)(H)\right]^- + H_2O \rightarrow \left[U^{VI}O_2(O)(OH)\right]^- + H_2 \quad (3)$$

The product ion at *m/z* 321, which is 18 units higher in *m/z* than the *m/z* 303 peak, may either be an H_2O adduct (formally $[U^{VI}O_2(O)(OH)(H_2O)]^-$) that appears at long isolation times, or a *tris*-hydroxy species $[U^{VI}O_2(OH)_3]^-$. Determination of the true composition and structure for this species would benefit from an IRMPD investigation. Subsequent CID of the ion at *m/z* 321 caused elimination of H_2O to re-form the species at *m/z* 303 (spectrum not shown), a pathway that could be possible for either species.

Although the reaction of $[U^{VI}O_2(O)(H)]^-$ with H_2O has not yet been reported, the products generated by exposure of the similar species UO_3^- to CH_3OH in the gas phase has been investigated [39]. The results of most reactions between "uranate" species and CH_3OH involved elimination of $CH_2{=}O$ and H_2O. However, for some product ions, particularly those that potentially contained hydride ligands, H_2 elimination reactions reminiscent of those observed here for $[U^{VI}O_2(O)(H)]^-$ were observed.

It is important to note that an O_2 adduct to the $[U^{VI}O_2(O)(H)]^-$ ion, which would appear at *m/z* 319, was not observed even at

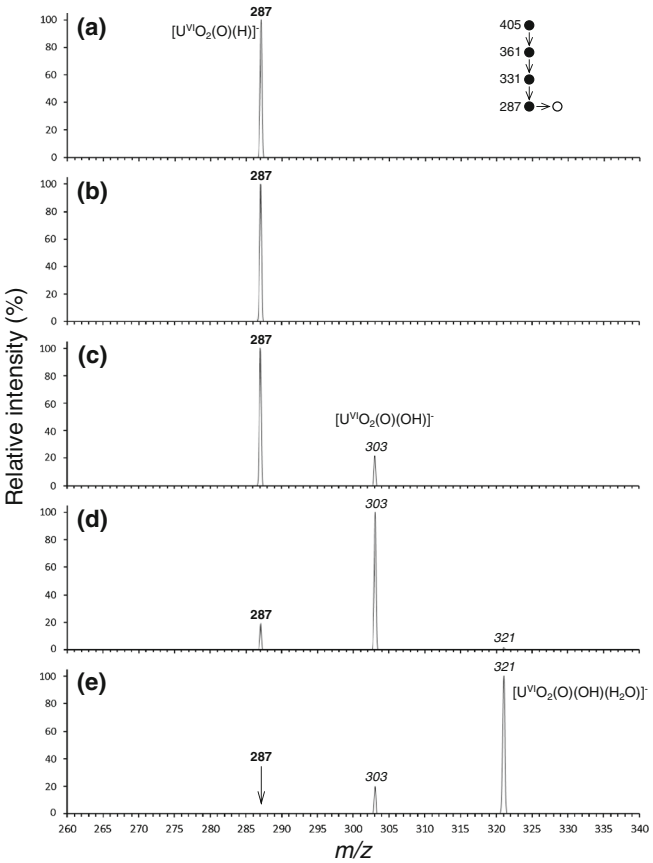

Figure 2. Product ion spectra (MS^5 stage) generated by isolation and storage of $[U^{VI}O_2(O)(H)]^-$, *m/z* 287, without imposed collisional activation, for reaction with background H_2O. Spectra were generated using isolation/reaction times of: (**a**) 1 ms, (**b**) 10 ms, (**c**) 100 ms, (**d**) 1 s, and (**e**) 10 s. In the spectrum, the circles and vertical arrows illustrate MS^n dissociation pathway. Horizontal arrows indicate ion-molecule reaction steps. The bold peak labels indicate the precursor selected for CID whereas labels in italics represent the products from dissociation or ion-molecule reactions as indicated in the text

isolation/reaction times as long at 10 s. Earlier studies have shown that cationic $U^VO_2^+$ complexes will reversibly bind molecular O_2, whereas $U^{VI}O_2^{2+}$ species do not [32–34]. Similar behavior with respect to O_2 addition has since been demonstrated for negatively charged species that contain $U^VO_2^+$ [35]. The tendency to add O_2 in an ion-molecule reaction can, therefore, be used to reveal those species that formally contain a $U^VO_2^+$ core. The fact that the anion at *m/z* 287 in the present study does not add O_2 strongly suggests that it contains a $U^{VI}O_2^{2+}$ core, and supports our composition assignment.

Isolation of the species at *m/z* 331 (attributed to formation of $[U^{VI}O_2(O)(O_2C\text{-}H)]^-$ in Figure 1b and c) to react with H_2O was also investigated. The only product observed, however, was an apparent H_2O adduct using isolation times ranging from 1 ms to 10 s (product ion spectra using isolation times of 1 ms to 1 s are provided in Supplementary Figures S2a–d). As for the product generated by reaction of $[U^{VI}O_2(O)(OH)]^-$ with H_2O, the composition and structure of the peak at *m/z* 349 is difficult

to assign unambiguously. The species may be a simple H_2O adduct (i.e., $[U^{VI}O_2(O)(O_2C\text{-}H(H_2O)]^-$), or a di-hydroxy species such as $[U^{VI}O_2(OH)_2(O_2C\text{-}H)]^-$. Subsequent CID of the ion at *m/z* 349 caused simple H_2O elimination (Supplementary Figure S2e). As for the *m/z* 287 species, no O_2 adduct was observed for the *m/z* 331 ion, suggesting that the anion also contains a $U^{VI}O_2^{2+}$ core coordinated by formate and oxide ligands.

The ion-molecule reactivity of the product ion at *m/z* 361, generated by elimination of CO_2 from $[U^{VI}O_2(O_2C\text{-}H)_3]^-$, was more interesting. Although no products attributable to an ion-molecule reaction were observed at 1 ms isolation/reaction time, as shown in Figure 3, isolation of the species for 10 ms through 10 s (Figure 3a–d, respectively) and reaction with H_2O led to formation of an ion at *m/z* 377. This species is assigned as a $U^{VI}O_2^{2+}$ complex with hydroxide and formate, with corresponding elimination of H_2, generated via Reaction 4.

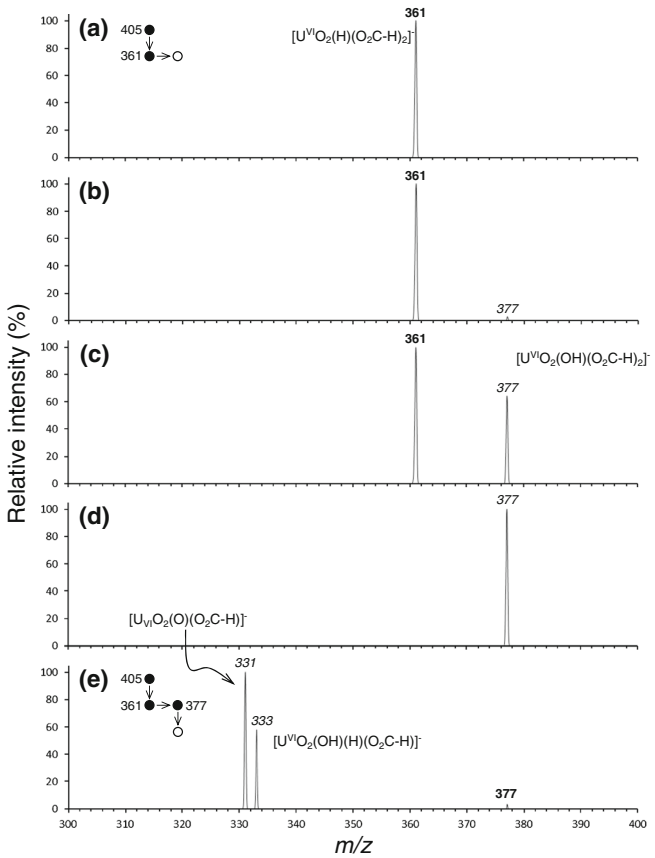

Figure 3. Product ion spectra generated by isolation and storage of $[U^{VI}O_2(H)(O_2C\text{-}H)_2]^-$, *m/z* 361, without imposed collisional activation, for reaction with background H_2O. Spectra in (a)–(**d**) are for isolation times of 1 ms, 10 ms, 1 s, and 10 s, respectively. The spectrum in (**e**) shows the product ions generated by CID of the *m/z* 377 ion. In the spectrum, the circles and vertical arrows illustrate MS^n dissociation pathway. Horizontal arrows indicate ion-molecule reaction steps. The bold peak labels indicate the precursor selected for CID whereas labels in italics represent the products from dissociation or ion-molecule reactions as indicated in the text

$$[U^{VI}O_2(H)(O_2C{-}H)_2]^- + H_2O \rightarrow [U^{VI}O_2(OH)(O_2C{-}H)_2]^- + H_2 \quad (4)$$

Product ions at *m/z* 333 and 331 were observed after subsequent CID of the ion at *m/z* 377 (MS^4 stage, Figure 3e). The product ion at *m/z* 331 exhibited the same ion-molecule reactivity as discussed above (and shown in Supplementary Figure S2a–e), leading to the conclusion that it is $[U^{VI}O_2(O)(O_2C\text{-}H)]^-$ generated by intra-complex proton transfer and elimination of (neutral) formic acid by Reaction 5.

$$[U^{VI}O_2(OH)(O_2C{-}H)_2]^- \rightarrow [U^{VI}O_2(O)(O_2C{-}H)]^- + HO_2C{-}H \quad (5)$$

The product ion at *m/z* 333 (generated by CID of $[U^{VI}O_2(OH)(O_2C\text{-}H)_2]^-$ at *m/z* 377) is formed by elimination of 44 mass units (CO_2), and likely represents the creation of $[U^{VI}O_2(OH)(H)(O_2CH)]^-$ by Reaction 6a. Subsequent CID of the ion at *m/z* 333 generated the species at *m/z* 331 (spectrum not shown) by elimination of H_2. Isolation of the product ion at *m/z* 333 for 1 s, without imposed collision activation (Supplementary Figure S3a), led to the generation of a peak at *m/z* 349 (16 mass units higher), and likely represents formation of a dihydroxy species through reaction with H_2O as shown in Reaction 6b. Subsequent CID of the *m/z* 349 ion (Supplementary Figure S3b) caused elimination of 18 mass units (presumably H_2O through Reaction 6c) to create the *m/z* 331 ion, for which the ion-molecule reaction behavior was identical to that described above.

$$[U^{VI}O_2(OH)(O_2C{-}H)_2]^- \rightarrow [U^{VI}O_2(OH)(H)(O_2C{-}H)]^- + CO_2 \quad (6a)$$

$$[U^{VI}O_2(OH)(H)(O_2C{-}H)]^- + H_2O \rightarrow [U^{VI}O_2(OH)_2(O_2C{-}H)]^- + H_2 \quad (6b)$$

$$[U^{VI}O_2(OH)_2(O_2C{-}H)]^- \rightarrow [U^{VI}O_2(O)(O_2C{-}H)]^- + H_2O \quad (6c)$$

No O_2 adducts to the ions at *m/z* 333, 349. or 377 were observed with isolation/reaction times up to 10 s, suggesting that each contains a $U^{VI}O_2^{2+}$ (i.e., U^{VI}) core.

Tandem MS of $[UO_2(O_2C\text{-}H)(CH_3CH_2OH)_2]^+$

The positive ion mass spectrum derived from uranyl-formate in H_2O/CH_3CH_2OH is shown in Figure 4a. The most abundant positively charged species generated by ESI appeared at *m/z* 407 and was initially assigned as $[U^{VI}O_2(O_2C\text{-}H)(CH_3CH_2OH)_2]^+$. However, because formate and ethoxide have the same nominal mass, the species could also be assigned the composition $[U^{VI}O_2(OCH_2CH_3)(CH_3CH_2OH)_2]^+$. The dominant pathways for the multiple-stage CID of the *m/z* 407 precursor (MS/MS and MS^3 stages, Figure 4b and c) involved elimination of single CH_3CH_2OH ligands, leading ultimately to a product ion at *m/z*

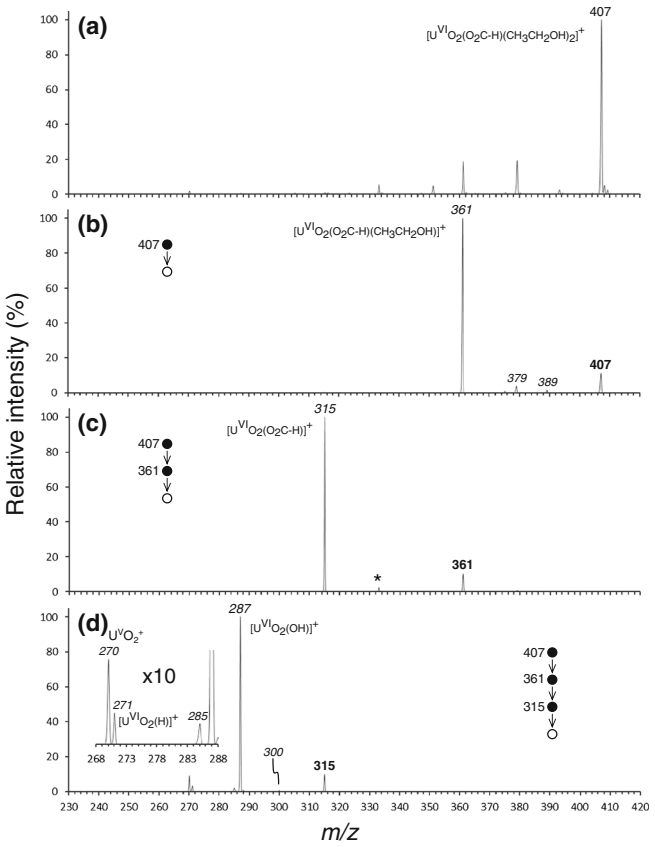

Figure 4. Positive ESI and CID spectra derived from uranyl formate in 50/50 H_2O/CH_3CH_2OH: (**a**) Full ESI spectrum, (**b**) CID of $[U^{VI}O_2(O_2C\text{-}H)(CH_3CH_2OH)_2]^-$ at *m/z* 407, (**c**) CID (MS^3 stage) of CID of $[U^{VI}O_2(O_2C\text{-}H)(CH_3CH_2OH)]^-$ at *m/z* 361, and (**d**) CID (MS^4 stage) of CID of $[U^{VI}O_2(O_2C\text{-}H)]^-$ at *m/z* 315. In the spectra, the circles and arrows illustrate the MS^n pathway. In each spectrum, the bold peak label indicates the precursor selected for CID whereas labels in italics represent the products from dissociation or ion-molecule reactions as indicated in the text

315 (Figure 4c). Minor peaks at *m/z* 379 and 389 were observed in the CID spectrum of $[U^{VI}O_2(O_2C\text{-}H)(CH_3CH_2OH)_2]^+$ (Figure 4b) that appear to involve the decomposition of CH_3CH_2OH into $CH_2{=}CH_2$ and H_2O were observed. Subsequent CID of these species generated the *m/z* 361 product ion that is the base peak in Figure 4b.

With the mass accuracy of the LIT used for these experiments, it is not possible to distinguish formate from ethoxide. However, assignment can be made with greater confidence by inspection of the CID pattern generated from the *m/z* 315 ion (Figure 4d). To begin with, we recently investigated the fragmentation of uranyl-methoxide and uranyl-ethoxide cations, $[U^{VI}O_2(OCH_3)]^+$ and $[U^{VI}O_2(OCH_2CH_3)]^+$ [40]. Our experiments demonstrated that $[U^{VI}O_2(OCH_3)]^+$ dissociates by reductive elimination of methoxy radical ($\bullet OCH_3$) to make $U^{V}O_2^+$, or by transfer of H^- from the methyl group to make $U^{VI}O_2H^+$. The $[U^{VI}O_2(OCH_2CH_3)]^+$ ion instead dissociates by pathways that involve the elimination or retention of CH_3 and CH_2O. The retention of CH_3 leads to a product ion at *m/z* 285, whereas retention of CH_2O creates a product ion at *m/z* 300: these specific product ions can, therefore, be considered diagnostic for a $[U^{VI}O_2(OCH_2CH_3)]^+$ precursor ion. As is clear from inspection of Figure 4d, product ions at *m/z* 285 and 300 appear at less than 5% relative intensity, which strongly suggests that the population of ions contributing to the peak at *m/z* 315 in Figure 4c does not include a significant fraction of $[U^{VI}O_2(OCH_2CH_3)]^+$. The *m/z* 315 product is, therefore, mostly uranyl-formate cation, $[UO_2(O_2C\text{-}H)]^+$.

The dominant product ion generated by CID of $[U^{VI}O_2(O_2C\text{-}H)]^+$ appears at *m/z* 287, which as a cation can be assigned the composition $[U^{VI}O_2(OH)]^+$. Formation of $[U^{VI}O_2(OH)]^+$ presumably involves intramolecular H atom transfer and elimination of CO via Reaction 7. We note that the *m/z* value of the product ion shifted by one mass unit to 288 for CID of the $[U^{VI}O_2(O_2C\text{-}D)]^+$ precursor ion, consistent with the proposed fragmentation reaction.

$$\left[U^{VI}O_2(O_2C{-}H)\right]^+ \rightarrow \left[U^{VI}O_2(OH)\right]^+ + CO \qquad (7)$$

No O_2 adduct was observed when the *m/z* 287 (or 288 derived from the d-labeled precursor) was isolated without imposed collision activation. This again suggests that the species contains a $U^{VI}O_2^{2+}$ core. Formation of $[U^{VI}O_2(OH)]^+$ by intramolecular H atom transfer was also observed as a minor pathway in our earlier investigation of the dissociation of $[U^{VI}O_2OCH_2CH_3]^+$ [40].

Tandem MS of $[UO_2(O_2C\text{-}CH_3)_3]^-$

The ESI-MS spectrum generated from the uranyl acetate solution is shown in Figure 5a. As for formate, ESI generated primarily $[U^{VI}O_2(O_2C\text{-}CH_3)_3]^-$ at *m/z* 447 and larger clusters containing UO_2^{2+} and acetate. The multiple-stage CID spectra generated by initially isolating $[U^{VI}O_2(O_2C\text{-}CH_3)_3]^-$ at *m/z* 447 are shown in Figure 5b–e. Data generated using deuterium-labeled acetic acid ($HO_2\text{-}CD_3$) are provided in Supplementary Figure S4a–e.

The dominant product ion generated by CID of $[U^{VI}O_2(O_2C\text{-}CH_3)_3]^-$ at *m/z* 447 appeared at *m/z* 388, through a neutral loss of 59 mass units. The *m/z* 388 product is, therefore, generated by a dissociation reaction that involves elimination of acetyloxyl radical, $CH_3CO_2\bullet$, and reduction of $U^{VI}O_2^{2+}$ to $U^{V}O_2^+$. A minor peak (less than 5% relative intensity) was observed at *m/z* 403, which corresponds to the elimination of CO_2 to create $[U^{VI}O_2(CH_3)(O_2C\text{-}CH_3)_2]^-$. Again, because of the low mass cutoff of the LIT in these experiments, the degree to which $[U^{VI}O_2(O_2C\text{-}CH_3)_3]^-$ dissociates to produce the acetate anion could not be determined.

The elimination of $CH_3CO_2\bullet$ and CO_2 from $[U^{VI}O_2(O_2C\text{-}CH_3)_3]^-$ at the MS/MS stage are consistent with earlier CID studies [26, 30], including an investigation of decarboxylation and synthesis of organometallic actinide (An) species performed using a 3-D quadrupole ion trap [26]. Of three possible CID pathways for $[An^{VI}O_2(O_2C\text{-}CH_3)_3]^-$, An = U, Np, and Pu, considered in the earlier study (decarboxylation, anion ligand

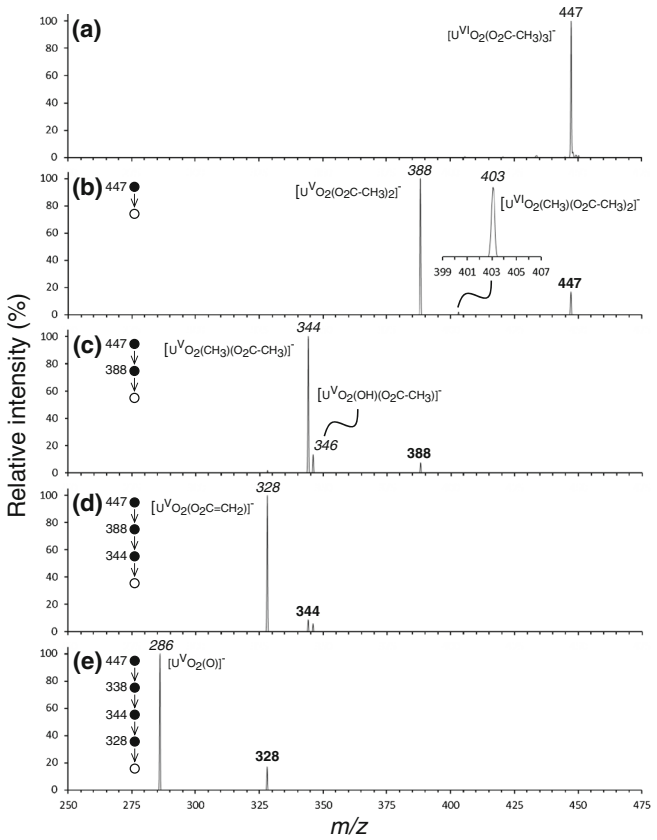

Figure 5. Negative ESI and CID spectra derived from uranyl acetate in 50/50 H_2O/CH_3CH_2OH: (**a**) Full ESI spectrum, (**b**) CID of $[U^{VI}O_2(O_2C\text{-}CH_3)_3]^-$ at *m/z* 447, (**c**) CID (MS^3 stage) of $[U^{V}O_2(O_2C\text{-}CH_3)_2]^-$ at *m/z* 388, (**d**) CID (MS^4 stage) of $[U^{V}O_2(CH_3)(O_2C\text{-}CH_3)]^-$ at *m/z* 344, and (**e**) CID (MS^5 stage) of $[U^{V}O_2(O_2C{=}CH_2)]^-$ at *m/z* 328. In the spectra, the circles and arrows illustrate the MS^n pathway. In each spectrum, the bold peak label indicates the precursor selected for CID whereas labels in italics represent the products from dissociation or ion-molecule reactions as indicated in the text

loss, and neutral ligand loss), the dominant CID channel was neutral ligand loss (elimination of acetyloxyl radical) to produce $[An^{V}O_2(O_2C\text{-}CH_3)_2]^-$. The CID reaction also leads to reduction of $An^{VI}O_2^{2+}$ to $An^{V}O_2^{+}$, and the favored dissociation pathway was consistent with DFT calculations of reaction energies.

CID of $[U^{V}O_2(O_2C\text{-}CH_3)_2]^-$ at *m/z* 388 (MS^3 stage, Figure 5b) caused the loss of 44 mass units (CO_2) to generate a product ion at *m/z* 344. The neutral loss was also 44 mass units following CID of the deuterium-labeled analogue, $[U^{V}O_2(O_2C\text{-}CD_3)_2]^-$ (Supplementary Figure S4c). The composition of the ion at *m/z* 344 is, therefore, assigned as $[U^{V}O_2(CH_3)(O_2C\text{-}CH_3)]^-$ ($[U^{V}O_2(CD_3)(O_2C\text{-}CD_3)]^-$ for the deuterium-labeled analogue). A minor peak at *m/z* 346 was also observed, the identity of which is discussed below.

Subsequent CID of the product ion at *m/z* 344 caused the elimination of 16 mass units, which we attribute to loss of CH_4, to leave an ion at *m/z* 328. The neutral loss at this CID stage shifted to 20 mass units for the deuterium labeled version of the precursor ion (Supplementary Figure S4d), demonstrating that the loss of methane involves intramolecular proton/deuteron transfer from an acetate ligand to the CH_3/CD_3 ligand. The product ion at *m/z* 328 is, therefore, assigned the composition $[U^{V}O_2(O_2C{=}CH_2)]^-$: $U^{V}O_2^{+}$ coordinated by an acetate enolate ligand. Subsequent CID of the *m/z* 328 ion generates a product ion at *m/z* 286, for which a composition assignment of $[U^{V}O_2(O)]^-$, created by elimination of ketene ($O{=}C{=}CH_2$), is reasonable. We note that there is precedent for products ions that are metal complexes with acetate enolate. For example, Meyer and coworkers reported the generation of lithium acetate enolate from malonic acid precursors using CID [41].

At this point, we can compare our CID results using the LIT to those of Luo et al. [30], who investigated the detection of uranyl species in natural water samples using extractive electrospray ionization and an instrument similar to the one employed in our study. In a discussion of the *intrinsic* fragmentation pathways for $[U^{VI}O_2(O_2C\text{-}CH_3)_3]^-$, the elimination of (neutral) $CH_3CO_2\bullet$ at the MS/MS stage to create $[U^{V}O_2(O_2C\text{-}CH_3)_2]^-$ at *m/z* 388 was noted, as was the relatively low abundance of the decarboxylation product at *m/z* 403. CID of $[U^{V}O_2(O_2C\text{-}CH_3)_2]^-$ was then reported to generate product ions at *m/z* 344 and 346 by elimination of 44 and 42 mass units, respectively, to leave $[U^{V}O_2(CH_3)(O_2C\text{-}CH_3)]^-$ and $[U^{V}O_2(OH)(O_2C\text{-}CH_3)]^-$. As we describe below, it is more likely that the latter product ion, $[U^{V}O_2(OH)(O_2C\text{-}CH_3)]^-$, is generated by a reaction of $[U^{V}O_2(CH_3)(O_2C\text{-}CH_3)]^-$ with H_2O after its generation by decarboxylation of $[U^{V}O_2(O_2C\text{-}CH_3)_2]^-$. In fact, there appear to be significant differences in the relative intensities of the *m/z* 344 and 346 product ions in our experiments compared with the earlier study by Luo and coworkers [30]. The *m/z* 346 ion is the base peak in the previous experiments, whereas the same ion appears at only 15% relative intensity in our experiments. The differences can probably be attributed to lower levels of adventitious H_2O in our experiment.

In the earlier study, CID of both the *m/z* 344 and 346 ions was reported to result in generation of product ions at *m/z* 302 and 304, which then ultimately dissociate to leave a terminal product ion at *m/z* 286 [30]. The *m/z* 286 product, assigned as $[U^{V}O_2(O)]^-$, is consistent with our experiments. However, the data shown here in Figure 5d indicate that under the conditions used in our study, the dominant dissociation pathway for the *m/z* 344 ion is the generation of the ion at *m/z* 328 through elimination of CH_4. The ions at *m/z* 302 and 304 are not observed as product ions from the dissociation of $[U^{V}O_2(CH_3)(O_2C\text{-}CH_3)]^-$. However, as we discuss below, both are observed as CID products of the *m/z* 346 product ion after it is generated by reaction of $[U^{V}O_2(CH_3)(O_2C\text{-}CH_3)]^-$ with H_2O.

As noted above, in our experiments the peak at *m/z* 346 was observed at ca. 15% relative intensity in the spectrum shown in Figure 5c. This peak is two mass units higher (the difference between CH_3 and OH) than the species at *m/z* 344, suggesting that $[U^{V}O_2(CH_3)(O_2C\text{-}CH_3)]^-$ (*m/z* 344) is hydrolyzed by reaction with background H_2O to generate $[U^{V}O_2(OH)(O_2C\text{-}$

$CH_3)]^-$ (*m/z* 346). Hydrolysis of $[U^VO_2(CH_3)(O_2C\text{-}CH_3)]^-$ to generate $[U^VO_2(OH)(O_2C\text{-}CH_3)]^-$ is consistent with the earlier study of actinyl-organometallic ions in the gas phase [26]. To test this hypothesis further, $[U^VO_2(CH_3)(O_2C\text{-}CH_3)]^-$ at *m/z* 344 was isolated and stored in the LIT for periods ranging from 1 ms to 10 s. The resulting product ion spectra are shown in Figure 6, and it is clear that with increasing isolation and reaction time there is a decrease in the relative intensity of the *m/z* 344 ion, and increase in the intensity of the ion at *m/z* 346. This strongly suggests that $[U^VO_2(OH)(O_2C\text{-}CH_3)]^+$ is generated from $[U^VO_2(CH_3)(O_2C\text{-}CH_3)]^-$ by Reaction 8.

$$\left[U^VO_2(CH_3)(O_2C{-}CH_3)\right]^- + H_2O \rightarrow \left[U^VO_2(OH)(O_2C{-}CH_3)\right]^+ + CH_4 \quad (8)$$

For isolation of $[U^VO_2(CD_3)(O_2C\text{-}CD_3)]^-$ (*m/z* 350, data not shown), reaction with H_2O generated $[U^VO_2(OH)(O_2C\text{-}CD_3)]^+$ at *m/z* 349, consistent with addition of OH and elimination of CD_3H.

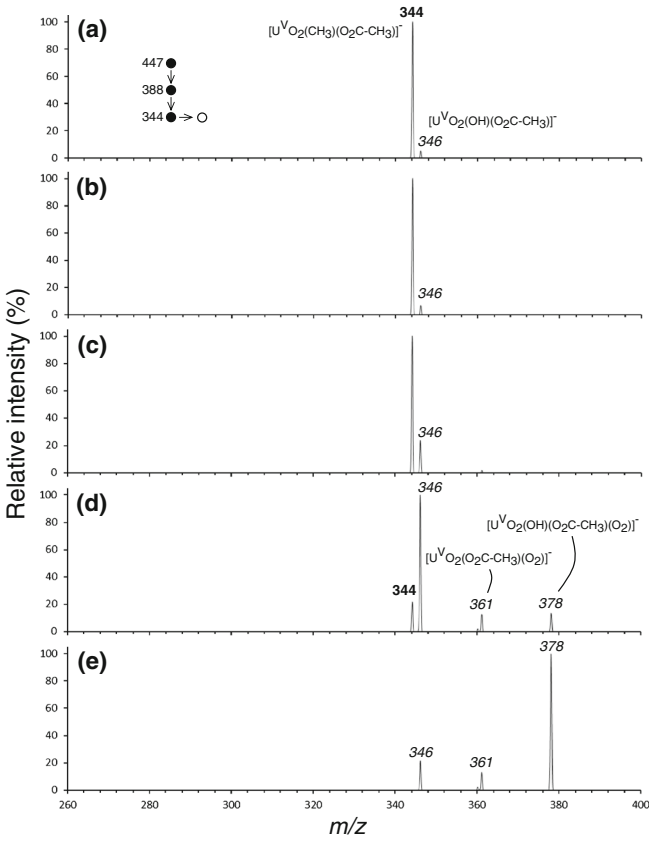

Figure 6. Product ion spectra (MS^5 stage) generated by isolation and storage of $[U^VO_2(CH_3)(O_2C\text{-}CH_3)]^-$, *m/z* 344, without imposed collisional activation, for reaction with background H_2O. Spectra were generated using isolation/reaction times of: (**a**) 1 ms, (**b**) 10 ms, (**c**) 100 ms, (**d**) 1 s, and (**e**) 10 s. In the spectrum, the circles and vertical arrows illustrate MS^n dissociation pathway. Horizontal arrows indicate ion-molecule reaction steps. The bold peak labels indicate the precursor selected for CID whereas labels in italics represent the products from dissociation or ion-molecule reactions as indicated in the text

Additional peaks at *m/z* 361 and 378 in Figure 6d and e represent the formation of the O_2 adducts $[U^VO_2(O_2C\text{-}CH_3)(O_2)]^-$ and $[U^VO_2(OH)(O_2C\text{-}CH_3)(O_2)]^-$. As noted in the discussion of product ions from the uranyl-formate system, formation of O_2 adducts is known to occur for complex ions that contain the reduced $U^VO_2^+$ core [32–35]. The appearance of the O_2 adducts in spectra shown in Figure 6d and e, therefore, demonstrate that both the *m/z* 344 and 346 ions contain $U^VO_2^+$ cores, as expected following the initial elimination of acetyloxyl radical from $[U^{VI}O_2(O_2C\text{-}CH_3)_3]^-$ (Figure 5a).

Subsequent isolation and CID of the presumed hydrolysis product, $[U^VO_2(OH)O_2C\text{-}CH_3)]^+$, generated several product ions (Supplementary Figure S5b). One appeared at *m/z* 328, representing the elimination of H_2O, presumably to generate $[U^VO_2(O_2C{=}CH_2)]^-$ as described above. Additional product ions from the CID of $[U^VO_2(OH)O_2C\text{-}CH_3)]^+$ included the species at *m/z* 304 and 302 (both species were noted as apparent dissociation products from the *m/z* 344 and 346 precursors by Luo et al. [30]). The former is assigned as $[U^VO_2(OH)_2]^-$, which presumably is generated via intramolecular proton transfer and elimination of O=C=CH_2. The latter ion is assigned as $[U^VO_2(O_2)]^-$. CID of the ion at *m/z* 302 (spectrum not shown) caused elimination of 16 mass units to generate $[U^VO_2(O)]^-$ at *m/z* 286.

Taken as a whole, the CID results reported here in Figure 5, and the ion-molecule reaction observations discussed above, provide a more accurate description of the intrinsic fragmentation pathways for the uranyl-acetate anion, $[U^{VI}O_2(O_2C\text{-}CH_3)_3]^-$. The primary fragmentation pathway for the intact precursor is elimination of acetyloxyl radical, $CH_3CO_2\bullet$, with reduction of $U^{VI}O_2^{2+}$ to $U^VO_2^+$. Subsequent CID of $[U^VO_2(O_2C\text{-}CH_3)_2]^-$ causes decarboxlation to generate $[U^VO_2(CH_3)(O_2C\text{-}CH_3)]^-$. Though some generation of $[U^VO_2(OH)(O_2C\text{-}CH_3)]^-$ (*m/z* 346) by elimination of 42 mass units cannot be ruled out as a CID pathway, our experiments suggest that the species is more likely formed by a reaction of $[U^VO_2(CH_3)(O_2C\text{-}CH_3)]^-$ with H_2O. CID of $[U^VO_2(CH_3)(O_2C\text{-}CH_3)]^-$ causes loss of CH_4 to create $[U^VO_2(O_2C{=}CH_2)]^-$, which subsequently fragments to generate $[U^VO_2(O)]^-$.

Tandem MS of $[UO_2(O_2C\text{-}CH_3)(CH_3CH_2OH)]^+$

The most abundant positively charged species generated by ESI of uranyl acetate dissolved in 50/50 H_2O/CH_3CH_2OH (data not shown) appeared at *m/z* 421 and was assigned as $[U^{VI}O_2(O_2C\text{-}CH_3)(CH_3CH_2OH)_2]^+$. CID of the *m/z* 421 precursor (MS/MS and MS^3 stages, Supplementary Figure S5a and b) caused elimination of single CH_3CH_2OH ligands to generate a product ion at *m/z* 329. Unlike the case for the formate analog, there was no ambiguity as to the assignment of the ion at *m/z* 329 as uranyl-acetate cation, $[U^{VI}O_2(O_2C\text{-}CH_3)]^+$. Subsequent CID of $[U^{VI}O_2(O_2C\text{-}CH_3)]^+$ generated a product ion at *m/z* 287, again assigned as $[U^{VI}O_2(OH)]^+$. The product ion shifted to *m/z* 288 when CID of $[U^{VI}O_2(O_2C\text{-}CD_3)]^+$ (Supplementary Figure S5e) was examined, again

suggesting a formation pathway that involves intramolecular H^+ transfer and elimination of O=C=CH_2 (O=C=CD_2 for the deuterium labeled analogue). Isolation of $[U^{VI}O_2(OH)]^+$ or $[U^{VI}O_2(OD)]^+$ for periods up to 10 s caused formation of only H_2O adducts (data not shown). The lack of O_2 adducts is indicative of the U^{VI} oxidation state.

Conclusions

To summarize, ESI, CID, and gas-phase ion-molecule reactions were used to make and characterize species derived from precursors composed of uranyl cation (UO_2^{2+}) coordinated by formate or acetate ligands. The low levels of adventitious H_2O in our linear ion trap allowed (1) the intrinsic dissociation pathways for both systems to be determined, and (2) the identification of apparent dissociation products that are better described as species generated by ion-molecule reactions.

Anionic complexes containing UO_2^{2+} and formate ligands fragment by decarboxylation and by elimination of CH_2=O, ultimately to produce an oxo-hydride species $[UO_2(O)(H)]^-$. Elimination of formyloxyl radical, with associated reduction of $U^{VI}O_2^{2+}$ to $U^{V}O_2^{+}$, was not observed. Product ions generated by CID, which include $[U^{VI}O_2(O)(H)]^-$ and $[U^{VI}O_2(OH)(O_2C\text{-}H)]^-$, undergo subsequent reactions that involve H_2O addition and elimination of H_2.

Our experiments allow for a revision of the intrinsic dissociation pathways for $[U^{VI}O_2(O_2\text{-}CH_3)_3]^-$. The primary fragmentation pathway for the intact precursor is elimination of acetyloxyl radical, CH_3CO_2•, with reduction of $U^{VI}O_2^{2+}$ to $U^{V}O_2^{+}$. Subsequent CID of $[U^{V}O_2(O_2C\text{-}CH_3)_2]^-$ causes decarboxlation to generate $[U^{V}O_2(CH_3)(O_2C\text{-}CH_3)]^-$. Though some formation of $[U^{V}O_2(OH)(O_2C\text{-}CH_3)]^-$ (*m/z* 346) by direct elimination of 42 mass units during CID is possible, our experiments suggest that the species is instead formed by a reaction of $[U^{V}O_2(CH_3)(O_2C\text{-}CH_3)]^-$ with H_2O. CID of $[U^{V}O_2(CH_3)(O_2C\text{-}CH_3)]^-$ causes loss of CH_4 to create $[U^{V}O_2(O_2C{=}CH_2)]^-$, which subsequently fragments to generate $[U^{V}O_2(O)]^-$. Loss of CH_4 occurs by an intra-complex H^+ transfer process that leaves UO_2^+ coordinated by acetate and acetate enolate anions. Subsequent dissociation step causes elimination of CH_2=C=O to furnish $[UO_2(O)]^-$. Elimination of CH_4 is also observed as a result of hydrolysis caused by ion-molecule reactions with H_2O.

For both systems, CID of the positively charged precursor $[U^{VI}O_2(O_2\text{-}C\text{-}R)(CH_3CH_2OH)_2]^+$, R = H, D, CH_3, or CD_3, causes elimination of CH_3CH_2OH ligands in successive dissociation stages. Using a comparison to the known fragmentation pattern of $[U^{VI}O_2(OCH_2CH_3)]^+$, CID of the *m/z* 315 product ion derived from $[U^{VI}O_2(O_2\text{-}C\text{-}H)(CH_3CH_2OH)_2]^+$ can be used to assign the composition as the uranyl-formate cation, $[UO_2(O_2C\text{-}H)]^+$ (rather than uranyl-ethoxide cation). CID of both $[UO_2(O_2C\text{-}H)]^+$ and $[UO_2(O_2C\text{-}CH_3)]^+$ generate $[U^{VI}O_2(OH)]^+$, presumably through intramolecular H transfer and elimination of (neutral) CO or CH_2=C=O for the formate and acetate precursors.

Acknowledgments

M.V.S acknowledges support for this work in the form of start-up funds from the Bayer School of Natural and Environmental Sciences and Duquesne University. Laboratory space renovation was made possible by support by the National Science Foundation through grant CHE-0963450. E.P. and N.P. acknowledge support from Duquesne University and the National Science Foundation (CHE-1221615 and CHE-1263279) for a summer undergraduate research. J.P. acknowledges support for independent research from the American Chemical Society (ACS) Project SEED program, the Spectroscopy Society of Pittsburgh, the Society for Analytical Chemists of Pittsburgh, and the Pittsburgh Section of the ACS.

References

1. Weigel, F.: In: Katz, J.J., Morss, L.R., Seaborg, G.T. (eds.) The Chemistry of the Actinide Elements, p. 169. Chapman and Hall, London (1986)
2. Greenwood, N.N., Earnshaw, A.: Chemistry of the Elements. Butterworth Heinemann, Oxford (1997)
3. Murphy, W.M., Shock, E.L.: In: Burns, P.C., Finch, R. (eds.) Uranium: Mineralogy, Geochemistry, and the Environment, p. 221. Mineralogical Society of America, Washington, DC (1999)
4. Brookins, D.G.: Geochemical Aspects of Radioactive Waste Disposal. Springer-Verlag, New York (1984)
5. Agnes, G.R., Horlick, G.: Electrospray mass spectrometry as a technique for elemental analysis: preliminary results. Appl. Spectrosc. **46**, 401–406 (1992)
6. Tsierkezos, N.G., Roithova, J., Schroder, D., Oncak, M., Slavicek, P.: Can electrospray mass spectrometry quantitatively probe speciation? Hydrolysis of uranyl nitrate studied by gas-phase methods. Inorg. Chem. **48**, 6287–6296 (2009)
7. Groenewold, G.S., Gianotto, A.K., Cossel, K.C., Van Stipdonk, M.J., Moore, D.T., Polfer, N., Oomens, J., de Jong, W.A., Visscher, L.: Vibrational spectroscopy of mass-selected $[UO_2(ligand)_n]^{2+}$ complexes in the gas phase: comparison with theory. J. Am. Chem. Soc. **128**, 4802–4813 (2006)
8. Groenewold, G.S., Oomens, J., de Jong, W.A., Gresham, G.L., McIlwain, M.E., Van Stipdonk, M.J.: Vibrational spectroscopy of anionic nitrate complexes of UO_2^{2+} and Eu^{3+} isolated in the gas phase. Phys. Chem., Chem. Phys. **10**, 1192–1202 (2008)
9. Groenewold, G.S., Van Stipdonk, M.J., de Jong, W.A., Oomens, J., Gresham, G.L., McIlwain, M.E., Gao, D., Siboulet, B., Visscher, L., Kullman, M., Polfer, N.: Infrared spectroscopy of dioxouranium(V) complexes with solvent molecules: effect of reduction. Chem. Phys. Chem. **9**, 1278–1285 (2008)
10. Groenewold, G.S., van Stipdonk, M.J., Oomens, J., de Jong, W.A., McIlwain, M.E.: The gas-phase bis-uranyl nitrate complex $[(UO_2)_2(NO_3)_5]^-$: infrared spectrum and structure. Int. J. Mass Spectrom. **308**, 175–180 (2011)
11. Pasilis, S., Somogyi, Á., Herrmann, K., Pemberton, J.E.: Ions generated from uranyl nitrate solutions by electrospray ionization (ESI) and detected with fourier transform ion-cyclotron resonance (FT-ICR) mass spectrometry. J. Am. Soc. Mass Spectrom. **17**, 230–240 (2006)
12. Pasilis, S.P., Pemberton, J.E.: Speciation and coordination chemistry of uranyl(VI)-citrate complexes in aqueous solution. Inorg. Chem. **42**, 6793–6800 (2003)
13. Rios, D., Schoendorff, G., Van Stipdonk, M.J., Gordon, M.S., Windus, T.L., Gibson, J.K., de Jong, W.A.: Roles of acetone and diacetone alcohol in coordination and dissociation reactions of uranyl complexes. Inorg. Chem. **51**, 12768–12775 (2012)
14. Schoendorff, G., de Jong, W.A., Van Stipdonk, M.J., Gibson, J.K., Rios, D., Gordon, M.S., Windus, T.L.: On the formation of "hypercoordinated" uranyl complexes. Inorg. Chem. **50**, 8490–8493 (2011)
15. Van Stipdonk, M.J., Chien, W., Anbalagan, V., Bulleigh, K., Hanna, D., Groenewold, G.S.: Gas-phase complexes containing the uranyl ion and acetone. J. Phys. Chem. A **108**, 10448–10457 (2004)

16. Van Stipdonk, M.J., Chien, W., Bulleigh, K., Wu, Q., Groenewold, G.S.: Gas-phase uranyl-nitrile complex ions. J. Phys. Chem. A **110**, 959–970 (2006)
17. Das, D., Kannan, S., Maity, D.K., Drew, M.G.B.: Steric effects on uranyl complexation: synthetic, structural, and theoretical studies of carbamoyl pyrazole compounds of the Uranyl(VI) ion. Inorg. Chem. **51**, 4869–4876 (2012)
18. Dau, P.D., Su, J., Liu, H.-T., Huang, D.-L., Li, J., Wang, L.-S.: Photoelectron spectroscopy and the electronic structure of the uranyl tetrachloride dianion: $UO_2Cl_4^{2-}$. J. Chem. Phys. **137**, 064315 (2012)
19. Dau, P.D., Su, J., Liu, H.-T., Liu, J.-B., Huang, D.-L., Li, J., Wang, L.-S.: Observation and investigation of the uranyl tetrafluoride dianion ($UO_2F_4^{2-}$) and its solvation complexes with water and acetonitrile. Chem. Sci. **3**, 1137–1146 (2012)
20. Li, W.-L., Su, J., Jian, T., Lopez, G.V., Hu, H.-S., Cao, G.-J., Li, J., Wang, L.-S.: Strong electron correlation in UO_2^-: a photoelectron spectroscopy and relativistic quantum chemistry study. J. Chem. Phys. **140**, 094306 (2014)
21. Su, J., Dau, P.D., Qiu, Y.-H., Liu, H.-T., Xu, C.-F., Huang, D.-L., Wang, L.-S., Li, J.: Probing the electronic structure and chemical bonding in tricoordinate uranyl complexes $UO_2X_3^-$ (X = F, Cl, Br, I): competition between Coulomb repulsion and U–X bonding. Inorg. Chem. **52**, 6617–6626 (2013)
22. Rios, D., Michelini, M.C., Lucena, A.F., Marçalo, J., Gibson, J.K.: On the origins of faster oxo exchange for uranyl(V) versus plutonyl(V). J. Am. Chem. Soc. **134**, 15488–15496 (2012)
23. Rios, D., Rutkowski, P.X., Shuh, D.K., Bray, T.H., Gibson, J.K., Van Stipdonk, M.J.: Electron transfer dissociation of dipositive uranyl and plutonyl coordination complexes. J. Mass Spectrom. **46**, 1247–1254 (2011)
24. Rios, D., Rutkowski, P.X., Van Stipdonk, M.J., Gibson, J.K.: Gas-phase coordination complexes of dipositive plutonyl, PuO_2^{2+}: chemical diversity across the actinyl series. Inorg. Chem. **50**, 4781–4790 (2011)
25. Rutkowski, P.X., Rios, D., Gibson, J.K., Van Stipdonk, M.J.: Gas-phase coordination complexes of $U^{VI}O_2^{2+}$, $Np^{VI}O_2^{2+}$, and $Pu^{VI}O_2^{2+}$ with dimethylformamide. J. Am. Soc. Mass Spectrom. **22**, 2042–2048 (2011)
26. Dau, P.D., Rios, D., Gong, Y., Michelini, M.C., Marçalo, J., Shuh, D.K., Mogamman, M., Van Stipdonk, M.J., Corcovilos, T.A., Martens, J.K., Oomens, J., Redlich, B., Gibson, J.K.: Synthesis and hydrolysis of uranyl, neptunyl, and plutonyl gas-phase complexes exhibiting discrete actinide-carbon bonds. Organometallics **35**, 1228–1240 (2016)
27. Van Stipdonk, M.J., del Carmen Michelini, M., Plaviak, A., Martin, D., Gibson, J.K.: Formation of bare UO_2^{2+} and NUO^+ by fragmentation of gas-phase uranyl-acetonitrile complexes. J. Phys. Chem. A **118**, 7838–7846 (2014)
28. Heinemann, C., Schwarz, H.: NUO^+, a new species isoelectronic to the uranyl dication UO_2^{2+}. Chem. Eur. J. **1**, 7–11 (1995)
29. Van Stipdonk, M.J., O'Malley, C., Plaviak, A., Martin, D., Pestok, J., Mihm, P.A., Hanley, C.G., Corcovilos, T.A., Gibson, J.K., Bythell, B.J.: Dissociation of gas-phase, doubly charged uranyl–acetone complexes by collisional activation and infrared photodissociation. Int. J. Mass Spectrom. **396**, 22–34 (2016)
30. Luo, M., Hu, B., Zhang, X., Peng, D., Chen, H., Zhang, L., Huan, Y.: Extractive electrospray ionization mass spectrometry for sensitive detection of uranyl species in natural water samples. Anal. Chem. **82**, 282–289 (2010)
31. Groenewold, G.S., de Jong, W.A., Oomens, J., van Stipdonk, M.: Variable denticity in carboxylate binding to the uranyl dication. J. Am. Soc. Mass Spectrom. **21**, 719–727 (2010)
32. Groenewold, G.S., Cossel, K.C., Gresham, G.L., Gianotto, A.K., Appelhans, A.D., Olson, J.E., Van Stipdonk, M.J., Chien, W.: Binding of molecular O_2 to di- and tri-ligated $[UO_2]^+$. J. Am. Chem. Soc. **128**, 3075–3084 (2006)
33. Bryantsev, V.S., Cossel, K.C., Diallo, M.S., Goddard III, W.A., de Jong, W.A., Groenewold, G.S., Chien, W., Van Stipdonk, M.J.: 2-Electron 3-atom bond in side-on (η_2) superoxo complexes: U(IV) and U(V) dioxo monocations J. Phys. Chem. A **112**, 5777–5780 (2008)
34. Leavitt, C.M., Bryantsev, V.S., de Jong, W.A., Diallo, M.S., Goddard III, W.A., Groenewold, G.S., Van Stipdonk, M.J.: Addition of H_2O and O_2 to acetone and dimethylsulfoxide ligated uranyl(V) dioxocations. J. Phys. Chem. A **113**, 2350–2358 (2009)
35. Lucena, A.F., Carretas, J.M., Marçalo, J., Michelini, M.C., Gong, Y., Gibson, J.K.: Gas-phase reactions of molecular oxygen with uranyl(V) anionic complexes—synthesis and characterization of new superoxides of uranyl(VI). J. Phys. Chem. A **119**, 3628–3635 (2015)
36. Kim, E.H., Bradforth, S.E., Arnold, D.W., Metz, R.B., Neumark, D.M.: Study of HCO_2 and DCO_2 by negative ion photoelectron spectroscopy. J. Chem. Phys. **103**, 7801–7814 (1995)
37. Clements, T.G., Continetti, R.E.: Predissociation dynamics of formyloxl radical studies by the dissociative photodetachment of HCO_2^-/DCO_2^- + hv → H/D + CO_2 + e^-. J. Chem. Phys. **115**(12):5345–5348 (2001)
38. Wang, X.-B., Woo, H.-K., Wang, L.-S., Minofar, B., Jungwirth, P.: Determination of the electron affinity of the acteyloxyl radical (CH_3COO) by low-temperature anion photoelectron spectroscopy and ab initio calculations. J. Phys. Chem. A **110**, 5047–5050 (2006)
39. Michelini, M.C., Marçalo, J., Russo, N., Gibson, J.K.: Gas-phase reactions of uranate ions, UO_2^-, UO_3^-, UO_4^-, and UO_4H^-, with methanol: a convergence of experiment and theory. Inorg. Chem. **49**, 3836–3850 (2010)
40. Van Stipdonk, M.J., Hanley, C., Perez, E., Pestok, J., Mihm, P., Corcovilos, T.A.: Collision-induced dissociation of uranyl-methoxide and uranyl-ethoxide cations: formation of UO_2H^+ and uranyl-alkyl product ions. Rapid Commun. Mass Spectrom. **30**, 1879–1890 (2016)
41. Meyer, M.M., Khairallah, G.N., O'Hair, R.A.J., Kass, S.R.: Gas-phase synthesis and reactivity of the lithium acetate enolate anion, $^-CH_2CO_2Li$. Angew. Chem. Int. Ed. **48**, 2934–2936 (2009)